

B meson leptonic decay constant with quenched lattice NRQCD

(JLQCD Collaboration)

K-I. Ishikawa^{a, b}, N. Yamada^a, S. Aoki^c, M. Fukugita^d, S. Hashimoto^b, N. Ishizuka^{c, e},
 Y. Iwasaki^{c, e}, K. Kanaya^{c, e}, T. Kaneda^c, S. Kaya^b, Y. Kuramashi^{b, f}, H. Matsufuru^a,
 M. Okawa^b, T. Onogi^a, S. Tominaga^b, N. Tsutsui^a, A. Ukawa^{c, e}, T. Yoshié^{c, e}

^a *Department of Physics, Hiroshima University, Higashi-Hiroshima, Hiroshima 739-8526, Japan*

^b *High Energy Accelerator Research Organization (KEK), Tsukuba, Ibaraki 305-0801, Japan*

^c *Institute of Physics, University of Tsukuba, Tsukuba, Ibaraki 305-8571, Japan*

^d *Institute for Cosmic Ray Research, University of Tokyo, Tanashi, Tokyo 188-8502, Japan*

^e *Center for Computational Physics, University of Tsukuba, Tsukuba, Ibaraki 305-8577, Japan*

^f *Department of Physics, Washington University, St. Louis, Missouri 63130, USA*

(April 26, 2024)

Abstract

We present a lattice NRQCD study of the B meson decay constant in the quenched approximation with emphasis given to the scaling behavior. The NRQCD action and the heavy-light axial current we use include all terms of order $1/M$ and the perturbative $O(\alpha_s a)$ and $O(\alpha_s/M)$ corrections. Using simulations at three value of couplings $\beta=5.7, 5.9$ and 6.1 on lattices of size $12^3 \times 32, 16^3 \times 48$ and $24^3 \times 64$, we find no significant a dependence in f_B if the $O(\alpha_s a)$ correction is included in the axial current. We obtain $f_B = 167(7)(15)$ MeV, $f_{B_s} = 191(4)(17)_{(-0)}^{(+4)}$ MeV and $f_{B_s}/f_B = 1.15(3)(1)_{(-0)}^{(+3)}$, with the first error being statistical, the second systematic, and the third due to uncertainty of strange quark mass, while quenching errors being not included.

PACS number(s): 12.38.Gc, 12.39.Hg, 13.20.He, 14.40.Nd

I. INTRODUCTION

Lattice QCD provides a promising approach for a first-principles calculation of the hadronic matrix elements of B meson relevant for a precision determination of the Cabibbo-Kobayashi-Maskawa (CKM) matrix elements. The most important matrix element is the B meson leptonic decay constant f_B : it is needed to determine V_{td} ; from the lattice technical point of view it is the simplest B meson matrix element calculable in lattice QCD with which one can study systematic errors associated with a lattice treatment of heavy quark.

The need for a careful examination of systematic errors stems from the fact that their magnitude for naive quark actions such as the Wilson action is of $O(aM)$ with M the heavy quark mass. Hence errors of this origin can exceed 100% for a typical lattice spacing of $a^{-1} \sim 2\text{GeV}$ used in present simulations. To overcome this problem, recent lattice studies of f_B [1] employ non-relativistic effective theory of QCD (NRQCD) [2] or a non-relativistic interpretation of the relativistic lattice quark action for heavy quarks [3].

NRQCD is an effective theory formulated as an expansion in \mathbf{D}/M where \mathbf{D} is the spatial covariant derivative which is of $O(\Lambda_{\text{QCD}})$ in the heavy-light system. For NRQCD one has to choose the coefficients of the expansion by imposing a matching condition with the full theory. This can be made using perturbation theory. In practice one has to truncate both non-relativistic expansion and perturbative expansion at some order so that the systematic error in NRQCD calculations is organized as a double expansion in Λ_{QCD}/M and the strong coupling constant α_s .

An additional source of systematic errors is the discretization error proportional to some power of $a\Lambda_{\text{QCD}}$. Since NRQCD is valid only when $aM > O(1)$, the continuum limit $a \rightarrow 0$ can not be taken. Therefore, removing discretization errors is more important in this formalism than in the usual relativistic formulations for which continuum extrapolations can in principle be made. For this reason, in many lattice NRQCD calculations, the correction terms to remove $a\Lambda_{\text{QCD}}$ and even $(a\Lambda_{\text{QCD}})^2$ errors were introduced.

Until recently the matching coefficients for the action [4–6] and the current operators [7] have been available only at one-loop level without operator mixing. This means that $O(\alpha_s\Lambda_{\text{QCD}}/M)$ and $O(\alpha_s a\Lambda_{\text{QCD}})$ errors had been left unremoved. Recently, Shigemitsu and Morningstar carried out a one-loop calculation necessary for an $O(\alpha_s\Lambda_{\text{QCD}}/M)$ and $O(\alpha_s a\Lambda_{\text{QCD}})$ improvement of the heavy-light axial vector current [8,9]. The first simulation including this improvement was performed by Ali Khan *et al.* [10,11], in which they pointed out that the $O(\alpha_s\Lambda_{\text{QCD}}/M)$ and $O(\alpha_s a\Lambda_{\text{QCD}})$ terms significantly affect the values of f_B .

The study of Ali Khan *et al.* [10,11] was made at a single lattice spacing corresponding to the inverse gauge coupling $\beta = 6/g^2 = 6.0$, and hence left open the important question of the lattice spacing dependence of f_B obtained with lattice NRQCD (in Refs. [12] Hein has calculated f_{B_s} at $\beta=5.7$ and discuss the scaling behavior by combining the result at $\beta=6.0$ of Ref. [11]). In this article we report on results of our systematic study concerning this question. Our simulations are carried out with the plaquette action for gluons at $\beta = 5.7, 5.9$ and 6.1 corresponding to the range of lattice spacing $a \sim 0.18 - 0.09\text{fm}$. For light quark we employ the $O(a)$ -improved Wilson (clover) action [13] with the tadpole improved one-loop value for the clover coefficient [14,15]. We investigate in detail the effect of one-loop improvement of the heavy-light axial vector current as a function of the lattice spacing. Our main results are obtained to $O(1/M)$, but the question of higher order corrections are

examined by comparing the results for the NRQCD action complete to $O(1/M^2)$.

This paper is organized as follows. In Sec. II we summarize the NRQCD action we use. In Sec. III improvement of the axial vector current is discussed, and our one-loop mixing coefficients are presented. Details of the simulations and our methods for extraction of the decay constant are given in Sec. IV together with numerical results. We discuss the effect of improvement in the static limit in Sec. V. Our results for f_B are presented in Sec. VI where a comparison is also made with those obtained with the relativistic formalism. In Sec. VII the hyperfine splitting of the B meson and the $B_s - B$ mass difference are given. Our conclusions are summarized in Sec. VIII.

II. LATTICE NRQCD ACTION

A. Form of action

Let us denote by $Q(t, \mathbf{x})$ the two-component heavy quark field. This field evolves in the time direction according to the action,

$$S = \sum_{t, \mathbf{x}} Q^\dagger(t, \mathbf{x}) [Q(t, \mathbf{x}) - K_t Q(t-1, \mathbf{x})]. \quad (1)$$

where the operator K_t specifies the evolution; our choice is

$$K_t = \left(1 - \frac{aH_0}{2n}\right)_t^n \left(1 - \frac{a\delta H}{2}\right)_t U_{4t-1}^\dagger \left(1 - \frac{a\delta H}{2}\right)_{t-1} \left(1 - \frac{aH_0}{2n}\right)_{t-1}^n, \quad (2)$$

Here subscripts represent the time slice at which Hamiltonian operators such as $(1 - aH_0/2n)$ act, and an integer n is introduced to avoid instability appearing in the evolution equation due to unphysical momentum modes [2]. We note that the ordering of terms in Eq. (2) is different from the one employed in [11]: the factor $(1 - a\delta H/2)$ is placed inside of $(1 - aH_0/2n)$ in our choice.

The leading order Hamiltonian H_0 is given by

$$H_0 = -\frac{\Delta^{(2)}}{2M_0}. \quad (3)$$

For the correction term δH , we consider two choices corresponding to the non-relativistic expansion to order $1/M$ (δH_I) or to order $1/M^2$ (δH_{II}), given by

$$\delta H_I = -c_1 \frac{g}{2M_0} \boldsymbol{\sigma} \cdot \mathbf{B}, \quad (4)$$

$$\begin{aligned} \delta H_{II} = & -c_1 \frac{g}{2M_0} \boldsymbol{\sigma} \cdot \mathbf{B} + c_2 \frac{ig}{8M_0^2} (\boldsymbol{\Delta}^{(\pm)} \cdot \mathbf{E} - \mathbf{E} \cdot \boldsymbol{\Delta}^{(\pm)}) \\ & - c_3 \frac{g}{8M_0^2} \boldsymbol{\sigma} \cdot (\boldsymbol{\Delta}^{(\pm)} \times \mathbf{E} - \mathbf{E} \times \boldsymbol{\Delta}^{(\pm)}) \\ & - c_4 \frac{(\boldsymbol{\Delta}^{(2)})^2}{8M_0^3} + c_5 \frac{a^2 \boldsymbol{\Delta}^{(4)}}{24M_0} - c_6 \frac{a(\boldsymbol{\Delta}^{(2)})^2}{16nM_0^2}. \end{aligned} \quad (5)$$

We refer to the two choices as NRQCD-I and NRQCD-II. We work with both Hamiltonians in parallel and compare their results in order to examine effects of truncation in the $1/M$ expansion. Various covariant differential operators in the Hamiltonian are defined in terms of the forward and backward derivatives $\Delta_\mu^{(+)}$ and $\Delta_\mu^{(-)}$ in the μ -th direction as $\Delta_\mu^{(\pm)} \equiv (\Delta_\mu^{(+)} + \Delta_\mu^{(-)})/2$, $\Delta_\mu^{(2)} \equiv \Delta_\mu^{(+)}\Delta_\mu^{(-)}$, $\Delta^{(2)} \equiv \sum_{i=1}^3 \Delta_i^{(2)}$, and $\Delta^{(4)} \equiv \sum_{i=1}^3 (\Delta_i^{(2)})^2$. The field strength operators \mathbf{B} and \mathbf{E} are constructed with the clover-leaf definition as in Ref. [2]. The bare heavy quark mass is denoted as M_0 , and c_i 's are parameters to describe the strength of each term.

The relativistic four-component field ψ_h is related to the effective field Q through the Foldy-Wouthuysen-Tani (FWT) transformation,

$$\psi_h(t, \mathbf{x}) = RQ(t, \mathbf{x}), \quad (6)$$

Here the transformation operator R is given by

$$\begin{aligned} R_{\text{I}} &= 1 - d_1 \frac{\boldsymbol{\gamma} \cdot \boldsymbol{\Delta}^{(\pm)}}{2M_0}, \\ R_{\text{II}} &= 1 - d_1 \frac{\boldsymbol{\gamma} \cdot \boldsymbol{\Delta}^{(\pm)}}{2M_0} + d_2 \frac{\Delta^{(2)}}{8M_0^2} \\ &\quad + d_3 \frac{g}{8M_0^2} \boldsymbol{\Sigma} \cdot \mathbf{B} - d_4 \frac{ig}{4M_0^2} \gamma_4 \boldsymbol{\gamma} \cdot \mathbf{E}, \end{aligned} \quad (7) \quad (8)$$

with $\Sigma^j = \text{diag}\{\sigma^j, \sigma^j\}$, and R_{I} (R_{II}) is to be used in conjunction with δH_{I} (δH_{II}) to achieve the desired accuracy in the $1/M$ expansion.

The coefficients c_i and d_i should be determined by matching the action to the continuum relativistic QCD action by either resorting to perturbation theory or estimating it non-perturbatively so as to reproduce the same theory in each order of the $1/M$ expansion. So far even perturbative results are not available for these coefficients. We adopt the tree-level value $c_i = 1$ and $d_i = 1$ in our work, applying, however, the mean-field improvement to all the link variables in the action and the FWT transformation with the replacement $U_\mu \rightarrow U_\mu/u_0$, where we take $u_0 = \langle \text{Tr}U_{\text{plaq}}/3 \rangle^{1/4}$ [16].

III. IMPROVEMENT OF THE CURRENT

To calculate the decay constant f_B , the heavy-light axial vector current in lattice NRQCD has to be matched to that in continuum QCD. For the overall renormalization factor Z_A this was first performed by Davies and Thacker [7] by perturbation theory to one-loop order. An important recent development made by Shigemitsu and Morningstar [8,9] is that the matching has been extended to $O(\alpha_s a \Lambda_{\text{QCD}})$ and $O(\alpha_s \Lambda_{\text{QCD}}/M)$. Since our choice of the action is slightly different from that used by the authors of Refs. [7,9], we have repeated the one-loop calculation for our NRQCD action.

Consider the axial vector current $A_{4\text{cont}}$ in the continuum. We demand that on-shell S matrix elements of the lattice axial current reproduce that of the continuum current up to $O(\mathbf{p})$ with \mathbf{p} the spatial momentum of the heavy or light quark. At one-loop level the relation takes the form

$$A_{4\text{cont}} = \left[1 + \alpha_s \rho_A^{(0)}\right] J_{\text{latt}}^{(0)} + \alpha_s \rho_A^{(1)} J_{\text{latt}}^{(1)} + \alpha_s \rho_A^{(2)} J_{\text{latt}}^{(2)}, \quad (9)$$

where the heavy-light lattice operators of dimension 3 and 4 are defined by

$$J_{\text{latt}}^{(0)} = \bar{\psi}_l \Gamma \psi_h, \quad (10)$$

$$J_{\text{latt}}^{(1)} = \frac{-1}{2M_0} \bar{\psi}_l \Gamma \boldsymbol{\gamma} \cdot \boldsymbol{\Delta}^{(\pm)} \psi_h, \quad (11)$$

$$J_{\text{latt}}^{(2)} = \frac{1}{2M_0} \bar{\psi}_l \boldsymbol{\gamma} \cdot \overleftarrow{\boldsymbol{\Delta}}^{(\pm)} \Gamma \psi_h, \quad (12)$$

with $\Gamma = \gamma_5 \gamma_4$ for the temporal axial vector current, and ψ_l and ψ_h denoting the light and heavy quark fields, respectively. We calculate the coefficients $\rho_A^{(i)}$ for NRQCD-I for heavy quark and the $O(a)$ -improved clover action [13] for the light quark. The use of clover action for the light quark is necessary to achieve the accuracy of $O(\alpha_s a)$ in matching the current. For renormalization of the continuum current we adopt the $\overline{\text{MS}}$ scheme using dimensional regularization with fully anti-commuting γ_5 . We also apply the tadpole improvement procedure [16] with the average plaquette for all link variables in the covariant derivative of the operators, (11) and (12), and with the critical hopping parameter for the wave function renormalization of the light quark fields consistently in both non-perturbative and perturbative calculations.

Numerical results for the coefficients $\rho_A^{(i)}$ are listed in Table I, and plotted in Figure 1 as a function of $1/aM_0$. For $\rho_A^{(0)}$ the difference $\rho_A^{(0)} - (1/\pi) \ln(aM_0)$ is shown since the coefficient of the leading operator $1 + \alpha_s \rho_A^{(0)}$, being the usual renormalization factor Z_A , contains a logarithmic term $(1/\pi) \ln(aM_0)$. The other coefficients $\rho_A^{(1)}$ and $\rho_A^{(2)}$ are divided by $2aM_0$. The filled symbols represent the values explicitly obtained with the static action [17]. We have confirmed that the infinite mass limit of $\rho_A^{(0)} - (1/\pi) \ln(aM_0)$ agrees with the static results of Borrelli and Pittori [18] and of Golden and Hill [19].

We observe that $\rho_A^{(1)}/2aM_0$ vanishes in the limit $aM \rightarrow \infty$, which tells us that the contribution of $\alpha_s \rho_A^{(1)} J_{\text{latt}}^{(1)}$ is of $O(\alpha_s \Lambda_{\text{QCD}}/M)$. This is expected since $J_{\text{latt}}^{(1)}$ involves a derivative of the heavy quark field. On the other hand, $\alpha_s \rho_A^{(2)} J_{\text{latt}}^{(2)}$ does not contain such a derivative, and $\rho_A^{(2)}/2aM_0$ remains finite in the static limit as seen in Figure 1. Thus its contribution contains terms of $O(\alpha_s a \Lambda_{\text{QCD}})$. This term is an analogue of the current improvement term of $O(\alpha_s a)$ for the light quark discussed in Ref. [15].

We add a remark that we have repeated the one-loop calculation for the action employed in Ref. [9], and numerically confirmed their results to a 3 digit accuracy.

IV. DETAILS OF THE SIMULATION

A. Run Parameters

We list our simulation parameters in Table II. Our simulations are carried out for three values of the coupling $\beta=5.7, 5.9$ and 6.1 using the standard plaquette action for gluons. The corresponding values of the lattice spacing a is about $0.18, 0.13$ and 0.09 fm, respectively, if determined from the string tension. We choose our spatial lattice size to be larger than 2 fm.

For heavy quark we take five values of the bare mass aM_0 for each β to cover a range of the physical heavy quark mass M between 2 GeV and 16 GeV. This wide range of heavy quark mass enables us to examine explicitly the $1/M$ dependence of f_B . The parameter n is chosen so as to satisfy the stability condition $n > 3/aM_0$.

For light quark we use the $O(a)$ -improved Wilson action [13] with the clover coefficient $c_{\text{sw}} = (1/u_0^3)[1 + 0.199\alpha_V(1/a)]$, which includes the $O(\alpha_s)$ correction calculated in Refs. [14,15]. Four values of the light quark hopping parameter κ are employed for extrapolation to the chiral limit (see Table II for numerical values).

In the quenched approximation the value of the strange quark mass m_s differs depending on whether m_K or m_ϕ is used as input. The value of m_s determined with m_ϕ is higher than that with m_K , and the discrepancy does not become smaller for smaller lattice spacings. We choose to calculate f_{B_s} for both m_s , and take their difference as a systematic error. The hopping parameters κ_s (κ_{s1} from m_K and κ_{s2} from m_ϕ) are also given in Table II.

The physical scale of lattice spacing a is fixed using the string tension $\sigma = 427$ MeV. Recent data of the string tension for the standard plaquette action are summarized in Ref. [20]. We adopt their parameterization to obtain the values of $1/a$ at our β .

B. Fitting procedure and data analysis

The method to extract the heavy-light decay constant is standard. We define a local and a smeared operator for the pseudoscalar channel by

$$O_P^L(t, \mathbf{x}) = \bar{\psi}_l(t, \mathbf{x})\gamma_5\psi_h(t, \mathbf{x}), \quad (13)$$

$$O_P^S(t, \mathbf{x}) = \sum_{\mathbf{y}} \bar{\psi}_l(t, \mathbf{x})\gamma_5\psi_h(t, \mathbf{y})\phi^{\text{SRC}}(|\mathbf{x} - \mathbf{y}|), \quad (14)$$

in the Coulomb gauge. For the smearing function we use the form $\phi^{\text{SRC}}(|\mathbf{x}|) = \exp(-a|\mathbf{x}|^b)$, with the parameters a and b chosen so as to reproduce the functional form of the heavy-light meson wave function measured in our simulations. We measure the two-point functions given by

$$C_{PP}^{\text{LS}}(t_f, t_i) = \sum_{\mathbf{x}_f} \langle O_P^L(t_f, \mathbf{x}_f) O_P^{\text{S}\dagger}(t_i, \mathbf{0}) \rangle, \quad (15)$$

$$C_{PP}^{\text{SS}}(t_f, t_i) = \sum_{\mathbf{x}_f} \langle O_P^S(t_f, \mathbf{x}_f) O_P^{\text{S}\dagger}(t_i, \mathbf{0}) \rangle, \quad (16)$$

$$C_{J^{(i)}P}^{\text{LS}}(t_f, t_i) = \sum_{\mathbf{x}_f} \langle J_{\text{latt}}^{(i)}(t_f, \mathbf{x}_f) O_P^{\text{S}\dagger}(t_i, \mathbf{0}) \rangle, \quad (17)$$

with the Dirichlet boundary condition in temporal direction. In this measurement the source is placed at the time slice $t_i=6$ (at $\beta=5.7$), 7 (5.9) and 16 (6.1). For the heavy-light meson with zero spatial momentum, $C_{J^{(1)}P}^{\text{LS}}(t_f, t_i)$ and $C_{J^{(2)}P}^{\text{LS}}(t_f, t_i)$ are identical by construction.

We fit the correlators to the exponential form,

$$C_{PP}^{\text{LS}}(t_f, t_i) \rightarrow Z_{PP}^{\text{LS}} \exp(-aE^{\text{bin}}(t_f - t_i)), \quad (18)$$

$$C_{PP}^{\text{SS}}(t_f, t_i) \rightarrow Z_{PP}^{\text{SS}} \exp(-aE^{\text{bin}}(t_f - t_i)), \quad (19)$$

$$C_{J^{(i)}P}^{\text{LS}}(t_f, t_i) \rightarrow Z_{J^{(i)}P}^{\text{LS}} \exp(-aE^{\text{bin}}(t_f - t_i)), \quad (20)$$

over a range of t where we find a plateau in the effective mass plot. Representative effective mass plots for $C_{PP}^{\text{LS}}(t_f, t_i)$, $C_{PP}^{\text{SS}}(t_f, t_i)$, $C_{J^{(0)}P}^{\text{LS}}(t_f, t_i)$, and $C_{J^{(1)}P}^{\text{LS}}(t_f, t_i)$ are shown in Figures 2 (3) for the case of the heaviest (lightest) quark masses at $\beta=6.1$. The signal is remarkably clean even for $C_{J^{(1)}P}^{\text{LS}}$ which includes a spatial differential operator. To constrain the fit as much as possible we take the binding energy E^{bin} to be common among the correlators. This is particularly necessary for a stable extraction of Z_{PP}^{SS} since the signal for $C_{PP}^{\text{SS}}(t_f, t_i)$ is much noisier than those for the others. We estimate statistical errors of the fitted parameters using the jackknife method with unit bin size. Statistical correlation of data between different time slices or between different mass parameters is neglected in the fitting.

C. Heavy-light Meson Mass

We calculate the pseudoscalar meson mass aM_P from a sum of the renormalized heavy quark mass and the binding energy E^{bin} through the formula

$$aM_P = Z_m aM_0 - E + aE^{\text{bin}}, \quad (21)$$

where E is the energy shift and Z_m the kinetic mass renormalization of the heavy quark.

The one-loop calculation of E and Z_m was first carried out by Davies and Thacker [4] and by Morningstar [5]. We repeat the calculation for our action NRQCD-I. We write the perturbative expansion of E , Z_m and the wave function renormalization Z_{2h} as

$$E = \alpha_s A, \quad (22)$$

$$Z_m = 1 + \alpha_s B, \quad (23)$$

$$Z_{2h} = 1 + \alpha_s C, \quad (24)$$

and list A , B , and C in Table I.

D. Heavy-light Decay Constant

The pseudoscalar meson decay constant f_P is constructed from the contribution of each operator $J_{\text{latt}}^{(i)}$ defined by

$$a^{3/2}(f_P \sqrt{M_P})^{(i)} = \frac{a^{3/2}}{\sqrt{M_P}} \langle 0 | J_{\text{latt}}^{(i)} | P \rangle = Z_{J^{(i)}P}^{\text{LS}} \sqrt{\frac{2}{Z_{PP}^{\text{SS}}}} \sqrt{1 - \frac{3\kappa}{4\kappa_{\text{crit}}}}, \quad (25)$$

where $\sqrt{1 - 3\kappa/4\kappa_{\text{crit}}}$ represents the tadpole-improved wave function normalization factor for light quark. Including the one-loop corrections, the decay constant is given by

$$a^{3/2}(f_P \sqrt{M_P}) = [1 + \alpha_s \rho_A^{(0)}] a^{3/2}(f_P \sqrt{M_P})^{(0)} + \sum_{i=1}^2 \alpha_s \rho_A^{(i)} a^{3/2}(f_P \sqrt{M_P})^{(i)}. \quad (26)$$

We note that $a^{3/2}(f_P \sqrt{M_P})^{(1)} = a^{3/2}(f_P \sqrt{M_P})^{(2)}$ holds in the rest frame of the heavy-light meson.

In Figures 4 and 5 we show aE^{bin} and $a^{3/2}(f_P \sqrt{M_P})^{(i)}$ as a function of $1/\kappa$ together with a linear (solid lines) and a quadratic (dotted lines) fit. We employ the linear fit for chiral

extrapolation since the difference between the linear and quadratic fits are negligibly small compared with the errors of the data. The linear fit is also used for an interpolation to the strange quark. The values of aE^{bin} and $a^{3/2}(f_P\sqrt{M_P})^{(i)}$ at $\kappa = \kappa_{\text{crit}}$ as well as those at κ_{s1} and κ_{s2} extracted in this way are summarized in Tables III, IV and V.

One of the points we discuss in detail below is the effect of $O(\alpha_s a \Lambda_{\text{QCD}})$ improvement in the static limit. For this purpose we need to extract the decay constant in the static limit.

Figure 6 shows the dependence of $(f_P\sqrt{M_P})^{(0)}$ as a function of $1/M_P$ for each β where M_P is calculated by the tree-level formula. The physical scale of lattice spacing a is determined from the string tension. We fit the mass dependence by

$$a^{3/2}(f_P\sqrt{M_P})^{(0)} = a^{3/2}(f_P\sqrt{M_P})^{(0)}\Big|_{\text{static}} \left(1 + \frac{a_1}{aM_P} + \frac{a_2}{(aM_P)^2} \right). \quad (27)$$

We also fit the mass dependence of $2aM_0a^{3/2}(f_P\sqrt{M_P})^{(1)}$ by

$$2aM_0a^{3/2}(f_P\sqrt{M_P})^{(1)} = 2aM_0a^{3/2}(f_P\sqrt{M_P})^{(1)}\Big|_{\text{static}} \left(1 + \frac{a'_1}{aM_P} + \frac{a'_2}{(aM_P)^2} \right). \quad (28)$$

Similarly, Figure 7 shows the $1/M_P$ dependence of the ratio $-2M_0(f_P\sqrt{M_P})^{(1)}/(f_P\sqrt{M_P})^{(0)}$. The functional dependence can also be parameterized as

$$-2aM_0 \frac{(f_P\sqrt{M_P})^{(1)}}{(f_P\sqrt{M_P})^{(0)}} = -2aM_0 \frac{(f_P\sqrt{M_P})^{(1)}}{(f_P\sqrt{M_P})^{(0)}}\Big|_{\text{static}} \left(1 + \frac{b_1}{aM_P} + \frac{b_2}{(aM_P)^2} \right). \quad (29)$$

The values of $a^{3/2}(f_P\sqrt{M_P})^{(0)}\Big|_{\text{static}}$ and $2aM_0a^{3/2}(f_P\sqrt{M_P})^{(1)}\Big|_{\text{static}}$ are given in Table IV and V, respectively.

To obtain the B meson decay constant at the physical B meson mass, we fit the $1/M_P$ dependence of the renormalized quantity $f_P\sqrt{M_P}$ in the renormalization group invariant form $\Phi_P \equiv [\alpha_s(M_P)/\alpha_s(M_B)]^{2/11} f_P\sqrt{M_P}$ instead of fitting the contribution of individual operators and summing the results.

V. STATIC LIMIT

We begin discussion of our results with the lattice spacing dependence of the decay constant in the static limit. This limit has the advantage that errors that depend on the heavy quark mass such as $O(\alpha_s \Lambda_{\text{QCD}}/M)$ vanish, and hence we can see the effect of $O(\alpha_s a \Lambda_{\text{QCD}})$ improvement more clearly.

According to the discussion in Sec. III, the contribution of $J_{\text{latt}}^{(1)}$ vanishes in the static limit. From Eq. (9), the matching relation in the static limit for the axial vector current is given by

$$A_{4\text{cont}} = \left[1 + \alpha_s \rho_{\text{static}}^{(0)} \right] J_{\text{static}}^{(0)} + \alpha_s \rho_{\text{static}}^{(\text{disc})} a J_{\text{static}}^{(\text{disc})}, \quad (30)$$

where $\rho_{\text{static}}^{(0)}$ and $J_{\text{static}}^{(0)}$ are the naive static limit (except anomalous dimension) of $\rho_A^{(0)}$ and $J_{\text{latt}}^{(0)}$. $\rho_{\text{static}}^{(\text{disc})}$ and $J_{\text{static}}^{(\text{disc})}$ are defined as

$$\rho_{\text{static}}^{(\text{disc})} = \lim_{aM_0 \rightarrow \infty} \rho_A^{(2)}/2aM_0, \quad (31)$$

$$aJ_{\text{static}}^{(\text{disc})} = \lim_{aM_0 \rightarrow \infty} 2aM_0 J_{\text{latt}}^{(2)}. \quad (32)$$

The numerical value of the matching coefficients in the static limit is given in Table I.

The decay constant is calculated from

$$f_{B(s)}^{\text{static}} \equiv (f_{P(s)} \sqrt{M_{P(s)}})|_{\text{static}} / \sqrt{M_{B(s)}} \quad (33)$$

with

$$\begin{aligned} & (f_P \sqrt{M_P}) \Big|_{\text{static}} \\ &= \left[1 + \alpha_s \rho_{\text{static}}^{(0)} \right] \left\{ (f_P \sqrt{M_P})^{(0)} \Big|_{\text{static}} \right\} + \alpha_s \rho_{\text{static}}^{(\text{disc})} \left\{ 2aM_0 (f_P \sqrt{M_P})^{(1)} \Big|_{\text{static}} \right\}. \end{aligned} \quad (34)$$

A nominal value of $M_0=4.5$ GeV is used for the heavy quark mass to evaluate the logarithm of $\rho_{\text{static}}^{(0)}$. For the strong coupling constant α_s we employ $\alpha_V(q^*)$ [16] evolved from $\mu = 3.40/a$ to q^* . Within one-loop calculations there is an uncertainty in the choice of the scale q^* . We take the average of results obtained with $q^* = \pi/a$ and with $1/a$, and consider the discrepancy from the two choices of q^* as an upper and lower bound for the error due to two-loop corrections in the renormalization factor.

Figure 8 shows the a dependence of the decay constant in the static limit f_B^{static} and $f_{B_s}^{\text{static}}$. Open symbols represent the results which are not corrected for the mixing effect of the operator $aJ_{\text{static}}^{(\text{disc})}$ (which corresponds to the static limit of $2aM_0 J_{\text{latt}}^{(2)}$), and filled symbols include this effect. Statistical errors are shown with solid bars, and uncertainties due to the choice of q^* by dotted bars. From the figure we see that an apparent a dependence for the unimproved results is removed by the inclusion of the higher dimensional operator $J_{\text{static}}^{(\text{disc})}$ at the one-loop level.

A worry with this observation is a sizable systematic error due to two-loop uncertainties. On this point we note that an estimate for the optimal value of q^* for the multiplicative renormalization coefficient is known to be $q^* = 2.18/a$ for the combination of the static heavy quark and the unimproved Wilson light quark [21]. Since there seems to be no obvious reason that this value changes significantly for the $O(a)$ -improved light quark action, taking the difference of the results for $q^* = \pi/a$ and $1/a$ may well be an overestimate of the two-loop uncertainty. An alternative estimate employing $\alpha_s(2/a)$ would reduce the error estimate by roughly a factor two. Furthermore the magnitude of this error is correlated among different β , and between results without and with the improvement at each β . Hence a reduction of the a dependence is less affected by the choice of q^* than $f_{B(s)}^{\text{static}}$ itself.

Numerically the magnitude of the $O(\alpha_s a)$ term relative to that of the leading operator $J_{\text{static}}^{(0)}$ (the static limit of $J_{\text{latt}}^{(0)}$) takes values,

$$\begin{aligned} & \alpha_s \times \rho_{\text{static}}^{(\text{disc})} \times 2aM_0 \frac{(f_P \sqrt{M_P})^{(1)}}{(f_P \sqrt{M_P})^{(0)}} \Big|_{\text{static}} \\ &= 0.272(84) \times 1.036 \times (-0.712(9)) = -0.201(84) \quad \text{at } \beta=5.7, \\ &= 0.217(53) \times 1.036 \times (-0.622(7)) = -0.140(53) \quad \text{at } \beta=5.9, \\ &= 0.189(40) \times 1.036 \times (-0.546(8)) = -0.107(41) \quad \text{at } \beta=6.1, \end{aligned} \quad (35)$$

where the error is dominated by the uncertainty in α_s . At $\beta = 6.1$ the effect reduces f_B^{static} by about 10% from the value without the improvement term.

VI. B MESON DECAY CONSTANT

A. Dependence on heavy-light meson mass

In Figure 9 we present $\Phi_P \equiv [\alpha_s(M_P)/\alpha_s(M_B)]^{2/11} f_P \sqrt{M_P}$ as a function of $1/M_P$ for three values of β of our simulation. Open symbols denote results from the leading operator alone, and filled symbols show how they change due to the inclusion of the higher dimensional operators $J_{\text{latt}}^{(1)}$ and $J_{\text{latt}}^{(2)}$. The factor $[\alpha_s(M_P)/\alpha_s(M_B)]^{2/11}$ is introduced to cancel the logarithmic divergence $(1/\pi) \ln(aM_0)$ in the one-loop coefficient $\rho_A^{(0)}$. For $\alpha_s(M_P)$ we use $\alpha_V(\mu)$ [16] evolved from $\mu = 3.40/a$ to M_P . The chiral limit is taken for the light quark. Solid and dotted error bars show the statistical error and the uncertainty due to two-loop corrections in the renormalization factors. The latter is estimated in the same way as for the static limit discussed in Sec. V.

As first observed in Refs. [8,10,11], the contributions from the operators $J_{\text{latt}}^{(1)}$ and $J_{\text{latt}}^{(2)}$ sizably affects the decay constant. The dominant effect arises from $J_{\text{latt}}^{(2)}$. A larger difference between the two sets of results toward the static limit is explained by the fact that the one-loop coefficient $\rho_A^{(2)}/2aM_0$ increases larger toward this limit (see Figure 1). In contrast, the contribution of $J_{\text{latt}}^{(1)}$ is negligible since the perturbative coefficient $\rho_A^{(1)}/2aM_0$ stays very small ($|\rho_A^{(1)}/2aM_0| < 0.2$) for our heavy quark mass $aM_0 > 1.2$.

As was the case for the decay constant in the static limit, uncertainties due to two-loop corrections are sizable, particularly at $\beta=5.7$. This uncertainty does decrease, however, for weaker couplings at $\beta = 5.9$ and 6.1 . It also becomes smaller as one moves down from the static limit toward the physical point for the B meson $M_P = M_B$.

B. Dependence on lattice spacing

By interpolating data shown in Figure 9 to the physical B meson mass, we obtain f_B for each β . The decay constant f_{B_s} for B_s meson is calculated in a similar manner. The bare b quark mass that reproduces the physical B meson mass is listed in Table VI, and f_B and f_{B_s} at each β are given in Table VII for the two choices of the scale $q^* = \pi/a$ and $1/a$.

The lattice spacing dependence of f_B and f_{B_s} is shown in Figure 10. Looking at the central values, we observe that a large a dependence exhibited by the results without the operator mixing (open symbols) is removed in the full result (filled symbols). This feature is clearer for f_{B_s} ; a variation is seen for f_B between $\beta = 5.9$ and 6.1 , albeit with simultaneously larger statistical errors. While we need to keep in mind the uncertainty due to a choice of α_s , this result indicates that the lattice spacing dependence of the B meson decay constant is sizably reduced after including the $O(\alpha_s a)$ and $O(\alpha_s/M)$ mixing terms.

C. Estimate of systematic errors

We now discuss possible sources of systematic errors and attempt an order estimate of their magnitude.

As already discussed the uncertainty from the scale for the strong coupling constant, which is an $O(\alpha_s^2)$ effect, is quite significant. The magnitude of this error, estimated as half the difference of values for $q^* = \pi/a$ and $1/a$ is given in Table VIII for each β .

We employ a light quark action which is $O(a)$ -improved at one-loop level. Since the two-loop uncertainty in this improvement of $O(\alpha_s^2 a \Lambda_{\text{QCD}})$ is negligibly small, we expect the leading discretization error from the light quark sector to be $O((a\Lambda_{\text{QCD}})^2)$, which is also the magnitude of scaling violation in the gluon sector. With a nominal value $\Lambda_{\text{QCD}} = 300$ MeV, we estimate its size to be 2%–8% depending on β as listed in Table VIII.

Our results are obtained for NRQCD-I which represents the leading term in an expansion in $1/M$. We examine possible corrections due to the truncation by explicitly comparing the results of NRQCD-I with those of NRQCD-II which is correct to $O(1/M^2)$. Figure 11 shows this comparison. We find that the $1/M^2$ correction does not exceed the statistical error, which is about 4% in the B meson mass region, as previously observed in Ref. [22]. Higher order uncertainties are expected to be even smaller.

Another source of the systematic error is the perturbative matching of the action and the operators of NRQCD. In the one-loop calculation of the self-energy and the current renormalization, we have consistently included all terms of order $1/M$. Hence $O(\alpha_s/(aM))$ corrections are properly taken into account in our calculation, and the leading error is of $O(\alpha_s/(aM)^2)$. An order estimate for $O(\alpha_s/(aM)^2)$ is given in Table VIII for each β . The magnitude increases for larger β since aM becomes smaller.

Adding these four leading systematic errors in quadrature, we find the systematic error to be about 8% at $\beta=6.1$ and 5.9, while it is much larger ($\sim 15\%$) at $\beta=5.7$. We, therefore, take an average over the two results at $\beta=6.1$ and 5.9 to quote our final result. In doing so, we have confirmed that the difference between 6.1 and 5.9 is within the estimated systematic error, as it should be.

In addition to the above systematic uncertainties, we must include an uncertainty in the lattice scale $1/a$. Throughout this work we have used the scale set with the string tension $\sqrt{\sigma}$. Taking a variation of the ratio $m_\rho/\sqrt{\sigma}$ over $\beta = 5.9, 6.1$ and 6.3, we assign a 3.5% error in the lattice scale as we did in Ref. [23].

D. Results

Our final result for the B meson decay constant in the quenched approximation is given by

$$f_B = 167(7)(15) \text{ MeV}, \quad (36)$$

$$f_{B_s} = 191(4)(17)_{(-0)}^{(+4)} \text{ MeV}. \quad (37)$$

Here the central value is an average over the results at $\beta=6.1$ and 5.9, and the errors are statistical and systematic in the given order. The systematic error includes 8% as estimated in the previous subsection and the error in the lattice scale of 3.5%, added in quadrature.

For f_{B_s} there is an additional uncertainty from the strange quark mass. We take the value from the K meson mass (κ_{s1}) for our central value. Employing the ϕ mass (κ_{s2}) gives a larger f_{B_s} , which is given in the final error.

Our result is higher than that of Ali Khan *et al.* [11] at $\beta=6.0$ ($f_B = 147(11)(16)$ MeV and $f_{B_s} = 175(8)(18)$ MeV), though consistent within one standard deviation. To compare with the results obtained with the the $O(a)$ -improved clover action, we quote from the studies of the Fermilab [24] group and of JLQCD [23],

$$\begin{aligned} f_B &= 164^{(+14)}_{(-11)}(8) \text{ MeV (Fermilab),} \\ &= 173(4)(13) \text{ MeV (JLQCD),} \\ f_{B_s} &= 185^{(+13)}_{(-8)}(9) \text{ MeV (Fermilab),} \\ &= 199(3)(14) \text{ MeV (JLQCD).} \end{aligned}$$

Our values with NRQCD are in good agreement with these relativistic calculations.

E. f_{B_s}/f_B

Many of systematic uncertainties that appear in the calculation of the pseudoscalar decay constant $f_{P_{(s)}}$ cancel, if we consider the ratio f_{P_s}/f_P . In particular, the two-loop uncertainty in the matching of the axial current cancels out explicitly.

Figure 12 presents the $1/M_P$ dependence of f_{P_s}/f_P . We observe only a mild $1/M_P$ dependence. The difference between NRQCD-I and NRQCD-II is much smaller than the statistical error, which shows that the contribution of the $1/M^2$ terms is negligible. Finally, plotting the ratio as a function of lattice spacing (see Figure 13), we find the results at three β values to be consistent with each other within the estimated errors.

Our result is

$$f_{B_s}/f_B = 1.15(3)(1)^{(+3)}_{(-0)}, \quad (38)$$

which is obtained by averaging data at $\beta=6.1$ and 5.9. The errors given are those from statistical, systematic and uncertainty in κ_s . For the systematic error the leading contribution arises from the lack of the strange quark mass dependent renormalization, which is $O(\alpha_s a \Lambda_{\text{QCD}})$ for the deviation $f_{B_s}/f_B - 1$. The magnitude is 3-5% assuming the order counting.

VII. MASS SPLITTINGS

A byproduct of our simulation is the mass difference between the B and B_s mesons, which can be compared with experiment. Since the heavy quark mass cancels in this difference, there are no direct perturbative corrections for this quantity, though they enter implicitly through determination of the bare b -quark mass.

We plot the $1/M_P$ dependence of the $B_s - B$ mass difference in Figure 14, where we observe the dependence to be small. The lattice spacing dependence is shown in Figure 15. A variation of about 20%, beyond the statistical error of 8%, is seen between the data at

$\beta=6.1$ and 5.9 , which may represent scaling violation effects. Our result from an average over $\beta=6.1$ and 5.9 is given by

$$M_{B_s} - M_B = 87(7)(4)_{(-0)}^{(+19)} \text{ MeV}, \quad (39)$$

where, as before, the errors represent statistical, systematic and κ_s uncertainty. The possible systematic error is $O((a\Lambda_{\text{QCD}})^2)$, which is 2-3%, and the uncertainty of $1/a \sim 3.5\%$. We estimate the error at 5% adding them in quadrature. The dominant error is the uncertainty of κ_s . It is encouraging that our result agrees with experimental value 90 ± 2 MeV.

The hyperfine splitting $M_{B^*} - M_B$ is another experimentally measured quantity. Previous lattice studies in the quenched approximation have found that the hyperfine splitting of heavy-light and heavy-heavy mesons are much smaller than experiment [25]. A possible reason for this discrepancy is an inappropriate value of the coupling c_1 for the $g\boldsymbol{\sigma} \cdot \mathbf{B}/2M_0$ term, for which we use the tadpole improved tree-level value. Since the hyperfine splitting of heavy-light mesons is proportional to c_1 , and that of heavy-heavy mesons to c_1^2 , it is possible that large corrections of $O(\alpha_s)$ remain (the non-perturbative calculation of this coupling has been done in Ref. [26], which reports the possible $O(\alpha_s)$ correction). Another possible source is the quenched approximation.

The $1/M_P$ dependence of the hyperfine splitting obtained in our simulation is shown in Figure 16. We observe that in the static limit the splitting linearly vanishes due to the heavy quark symmetry. Figure 17 shows the lattice spacing dependence of the splitting together with the experimental value of $M_{B^*} - M_B = 45.8 \pm 0.4$ MeV. While scaling is reasonably satisfied with our results, the magnitude is far below experiment. Averaging the two values at $\beta=6.1$ and 5.9 , we find

$$M_{B^*} - M_B = 23(7)(5) \text{ MeV}, \quad (40)$$

$$M_{B_s^*} - M_{B_s} = 26(3)(5)_{(-0)}^{(+1)} \text{ MeV}, \quad (41)$$

where we assume a 20% systematic error since the $O(\alpha_s)$ correction is not known for c_1 .

VIII. CONCLUSIONS

In this article we have presented a scaling study of the heavy-light meson decay constant using lattice NRQCD with the heavy-light current improved to $O(\alpha_s a)$ and to $O(\alpha_s/M)$ consistently to the one-loop order in perturbation theory taking into account mixings with the relevant higher dimensional operators. We have found the effect of the improvement to be substantial: the large a dependence of f_B is almost removed by the improvement. This is most apparent in the static limit, where the effect is purely $O(\alpha_s a)$, but a similar effect is also seen for the physical B mass.

The two main sources of systematic errors in our results are perturbative two-loop corrections, $O(\alpha_s^2)$, in the renormalization factors for the NRQCD action, $O(a)$ -improved Wilson action and the axial vector current, and the one-loop corrections of $O(\alpha_s/(aM)^2)$ in the coefficients of the NRQCD action and the axial vector current. The former uncertainty is quite large at $\beta = 5.7$, but diminishes to a 5% level at weaker couplings of $\beta = 5.9$ and 6.1 . The latter error, on the other hand, increases toward smaller lattice spacings, reaching $\sim 6\%$ at $\beta = 6.1$. This counter increase of error represents the limitation of lattice NRQCD

itself; the method breaks down once the heavy quark mass becomes smaller than the inverse lattice spacing.

The validity of a lattice NRQCD calculation of f_B hinges on the existence of a window in lattice spacing over which the two errors as well as scaling violations are small. We find these conditions to be satisfied at $\beta = 5.9 - 6.1$ where the combined systematic errors are estimated to be 8% (including the truncation in the $1/M$ expansion). Achieving better accuracy with NRQCD would require two-loop calculations to extend the window toward larger lattice spacings where the $O(\alpha_s/(aM)^2)$ error will become smaller.

Another method for calculating heavy quark quantities on the lattice is the non-relativistic interpretation of relativistic actions [3]. The advantage is that a continuum extrapolation can be carried out. The simulations by Refs. [23,24,27] have shown that the a dependence in the heavy-light decay constant is small for currently accessible range of $\beta = 5.7 \sim 6.3$. A continuum extrapolation, with either constant or linear fit in the lattice spacing, has yielded the decay constants with a systematic error of about 10%. A subtle point with this method, however, is that the a dependence of systematic errors is non-linear. Hence, strictly speaking, it is not correct to extrapolate the result with a simple linear or quadratic function of a . To achieve a prediction of the B meson decay constant more accurate than is available, one needs to improve the action and currents so that the systematic errors at finite values of β are further reduced. In this sense the study of $O(\alpha_s a)$ improvement should be necessary.

In spite of the limitations still inherent in the present results with NRQCD and with relativistic actions, we find it encouraging that the efforts with the two approaches have now yielded predictions for the B meson decay constant in mutual agreement within the total error of about 10% for quenched QCD.

ACKNOWLEDGMENT

This work is supported by the Supercomputer Project No.32 (FY1998) of High Energy Accelerator Research Organization (KEK), and also in part by the Grants-in-Aid of the Ministry of Education (Nos. 08640404, 09304029, 10640246, 10640248, 10740107, 10740125). K-I.I, S.K., H.M. and S.T. are supported by the JSPS Research Fellowship.

REFERENCES

- [1] For a recent review, see T. Draper, talk given at *Lattice '98* in Boulder, Colorado, July 1998, Nucl. Phys. **B** (Proc. Suppl.) (to be published), preprint hep-lat/9810065.
- [2] B. A. Thacker and G. P. Lepage, Phys. Rev. D **43**, 196 (1991); G. P. Lepage, L. Magnea, C. Nakhleh, U. Magnea, and K. Hornbostel, Phys. Rev. D **46**, 4052 (1992).
- [3] A. X. El-Khadra, A. S. Kronfeld, and P. B. Mackenzie, Phys. Rev. D **55**, 3933 (1997).
- [4] C. T. H. Davies and B. A. Thacker, Phys. Rev. D **45**, 915 (1992).
- [5] C. J. Morningstar, Phys. Rev. D **48**, 2265 (1993).
- [6] C. J. Morningstar, Phys. Rev. D **50**, 5902 (1994).
- [7] C. T. H. Davies and B. A. Thacker, Phys. Rev. D **48**, 1329 (1993).
- [8] J. Shigemitsu, Nucl. Phys. **B** (Proc. Suppl.) **60A**, 134 (1998); J. Shigemitsu and C. J. Morningstar, Nucl. Phys. **B** (Proc. Suppl.) **63A-C**, 341 (1998).
- [9] C. J. Morningstar and J. Shigemitsu, Phys. Rev. D **57**, 6741 (1998).
- [10] A. Ali Khan, J. Shigemitsu, S. Collins, C. T. H. Davies, C. Morningstar, and J. Sloan, Phys. Rev. D **56**, 7012 (1997).
- [11] A. Ali Khan, T. Bhattacharya, S. Collins, C. T. H. Davies, R. Gupta, C. J. Morningstar, J. Shigemitsu, and J. Sloan, Phys. Lett. **B427**, 132 (1998).
- [12] J. Hein, Nucl. Phys. **B** (Proc. Suppl.) **63A-C**, 347 (1998); talk given at *Lattice '98* in Boulder, Colorado, July 1998, preprint hep-lat/9809051; talk given at “Fourth Workshop on Quantum Chromodynamics” in The American University of Paris, France, June 1998, preprint hep-ph/9810314.
- [13] B. Sheikholeslami and R. Wohlert, Nucl. Phys. **B259**, 752 (1985).
- [14] R. Wohlert, DESY preprint 87-069 (1987); S. Naik, Phys. Lett. **B311**, 230 (1993).
- [15] M. Lüscher and P. Weisz, Nucl. Phys. **B479**, 429 (1996).
- [16] G. P. Lepage and P. B. Mackenzie, Phys. Rev. D **48**, 2250 (1993).
- [17] K-I. Ishikawa, T. Onogi, and N. Yamada, Phys. Rev. D (to be published), hep-lat/9812007.
- [18] A. Borrelli and C. Pittori, Nucl. Phys. **B385**, 502 (1992).
- [19] M. Golden and B. Hill, Phys. Lett. B **254**, 225 (1991).
- [20] R. G. Edwards, U. M. Heller, and T. R. Klassen, Nucl. Phys. **B517**, 377 (1998).
- [21] O. F. Hernandez and B. R. Hill, Phys. Rev. D **50**, 495 (1994).
- [22] K-I. Ishikawa, H. Matsufuru, T. Onogi, N. Yamada, and S. Hashimoto, Phys. Rev. D **56**, 7028 (1997).
- [23] JLQCD collaboration (S. Aoki *et al.*), Phys. Rev. Lett. **80**, 5711 (1998).
- [24] A. X. El-Khadra, A. S. Kronfeld, P. B. Mackenzie, S. M. Ryan, and J. N. Simone, Phys. Rev. D **58**, 014506 (1998).
- [25] C. T. H. Davies, Nucl. Phys. **B** (Proc. Suppl.) **60A**, 124 (1998); A. Ali Khan, Nucl. Phys. **B** (Proc. Suppl.) **63A-C**, 71 (1998)
- [26] H. D. Trottier and G. P. Lepage, Nucl. Phys. **B** (Proc. Suppl.) **63A-C**, 865 (1998).
- [27] C. Bernard *et al.*, Phys. Rev. Lett. **81**, 4812 (1998).

FIGURES

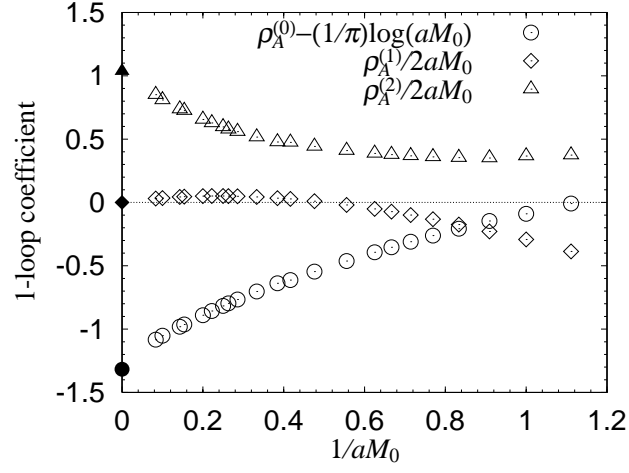


FIG. 1. $1/aM_0$ dependence of the one-loop coefficients for the axial vector current. Circles represent $\rho_A^{(0)} - 1/\pi \ln(aM_0)$. Diamonds and triangles are $\rho_A^{(1)}/2aM_0$ and $\rho_A^{(2)}/2aM_0$ respectively. The static limit is shown with the filled symbols.

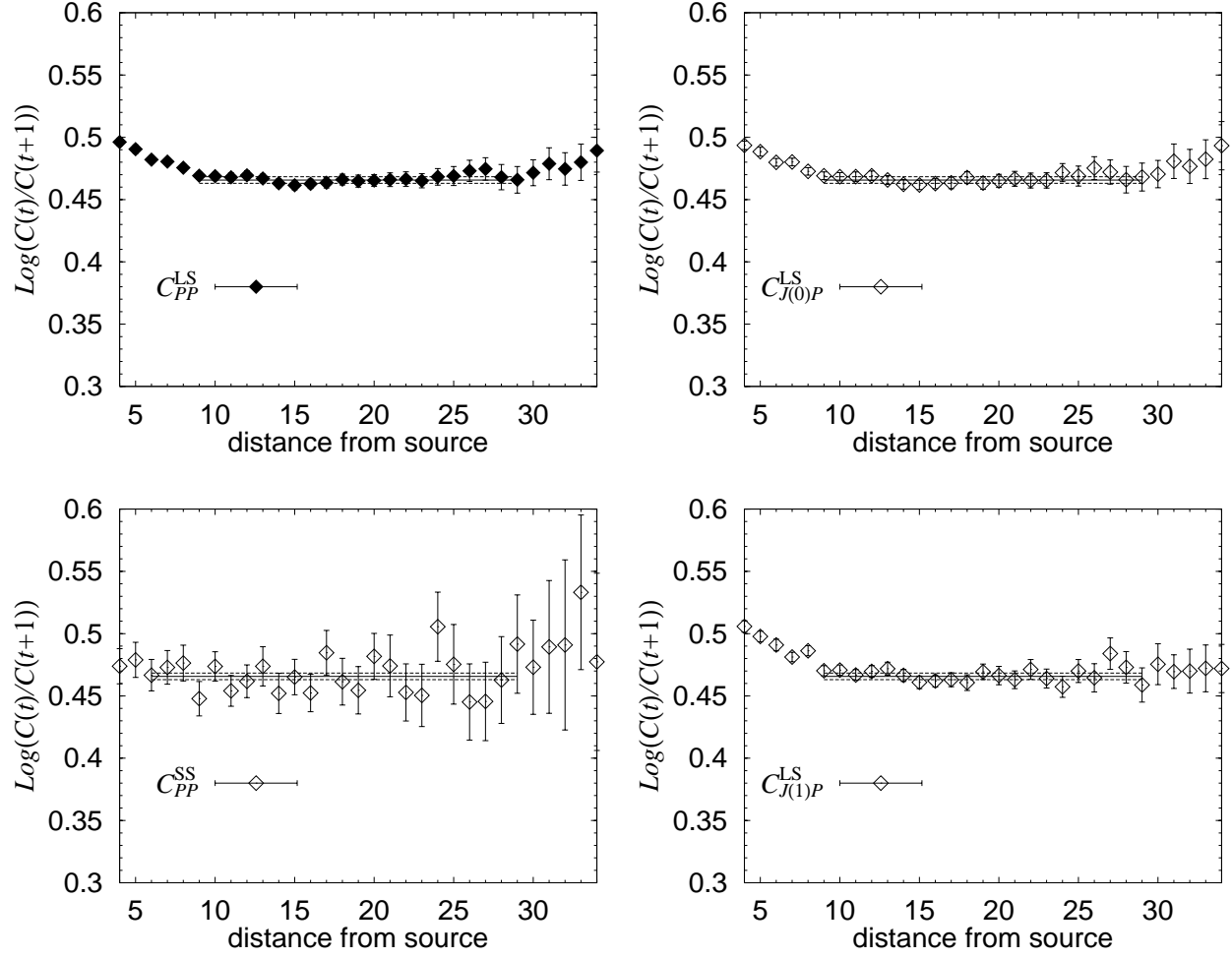


FIG. 2. Effective mass of various correlators at $\beta=6.1$ and $(aM_0, n) = (2.1, 2)$. The fitted value of aE^{bin} is shown by a solid line, and the error is indicated by dashed lines. The light quark hopping parameter $\kappa=0.13586$ is our heaviest one.

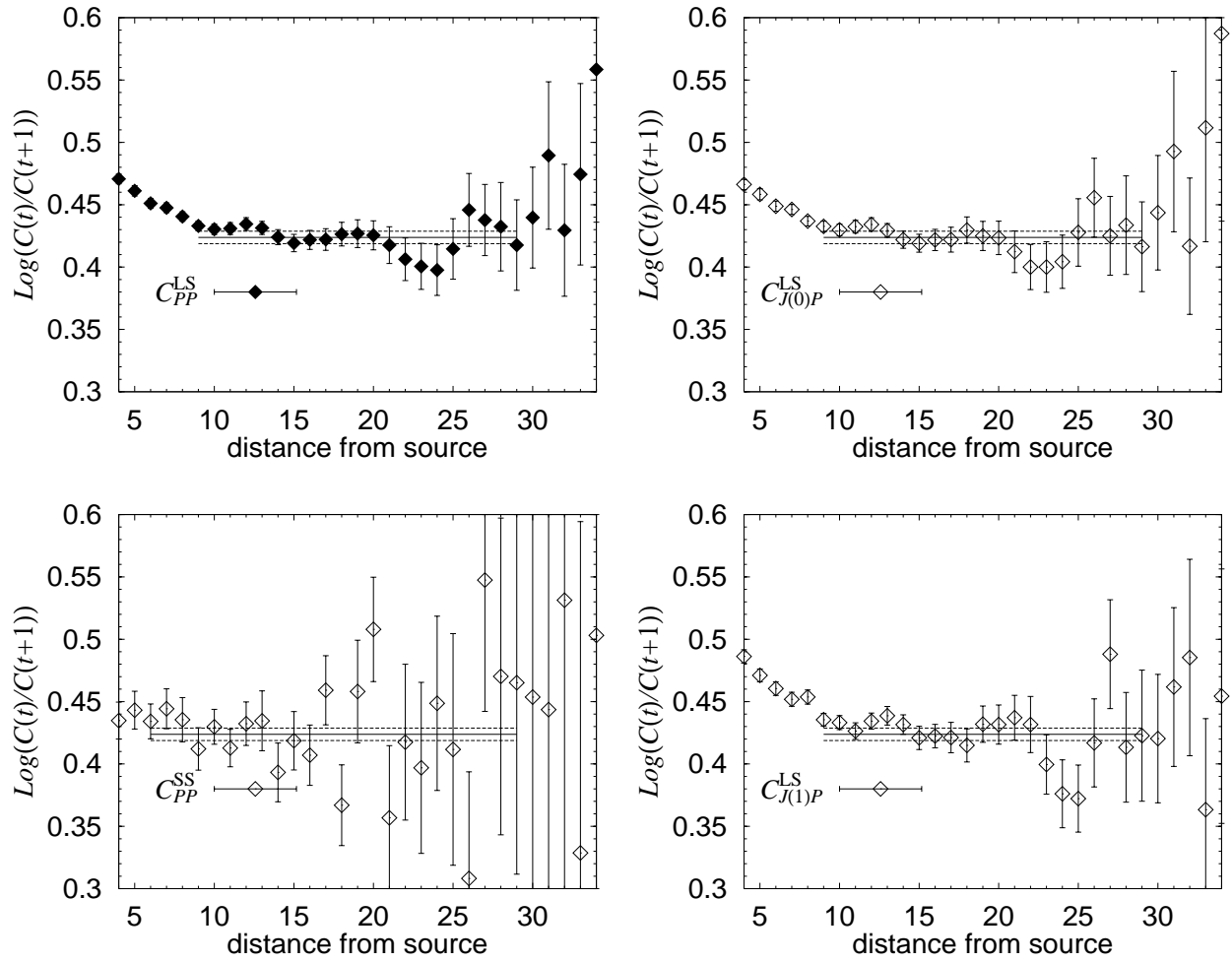


FIG. 3. Same as Figure 2, but with our lightest light quark mass $\kappa=0.13716$.

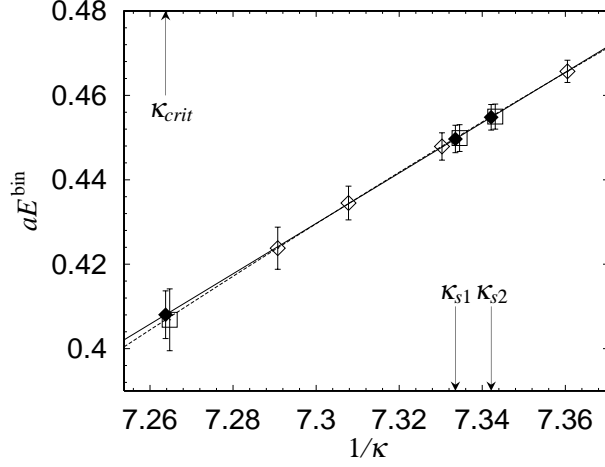


FIG. 4. Chiral limit of the heavy-light binding energy aE^{bin} at $\beta=6.1$ and $(aM_0, n) = (2.1, 2)$. Open diamonds represent our data. Filled diamonds are the results in the chiral limit (κ_{crit}) or in the strange quark mass (κ_{s1} or κ_{s2}) with linear fitting (solid line), and open squares are the results with quadratic fitting (dotted line).

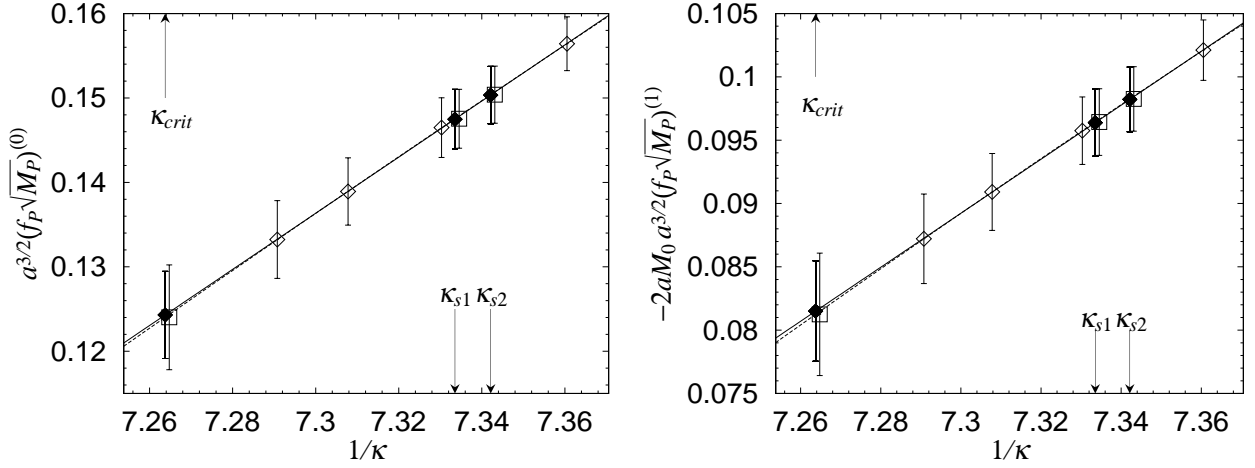


FIG. 5. Chiral limit of the decay constant $a^{3/2}(f_P\sqrt{M_P})^{(0)}$ (left) and $-2aM_0 a^{3/2}(f_P\sqrt{M_P})^{(1)}$ (right) at $\beta=6.1$ and $(aM_0, n) = (2.1, 2)$. The meaning of the symbols is the same as that in Fig. 4,

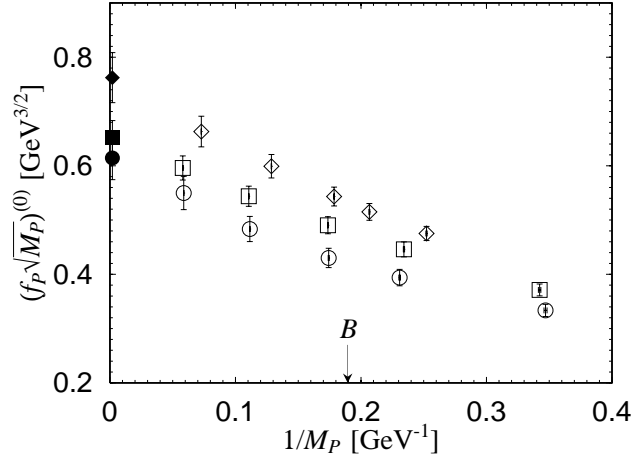


FIG. 6. $1/M_P$ dependence of $(f_P\sqrt{M_P})^{(0)}$. We used tree level value for M_P in the plot. Data at three β values are shown: $\beta=5.7$ (diamonds), 5.9 (squares), and 6.1 (circles). The static limit (filled symbols) is obtained with a quadratic extrapolation.

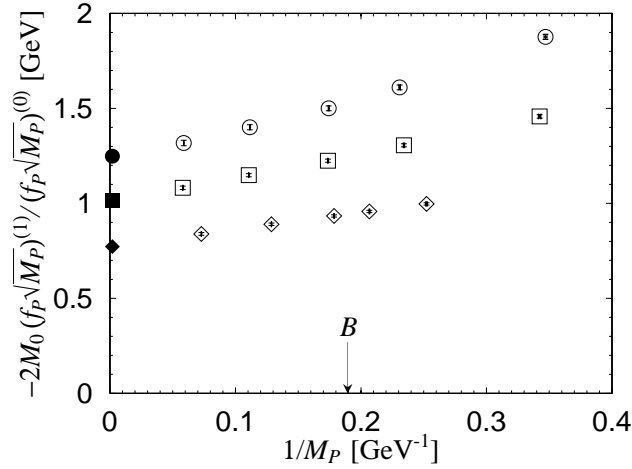


FIG. 7. Ratio of the leading and mixing operators $-2M_0(f_P\sqrt{M_P})^{(1)}/(f_P\sqrt{M_P})^{(0)}$. We used tree level results for $1/M_P$ in the plot. Data at three β values are shown: $\beta=5.7$ (diamonds), 5.9 (squares), and 6.1 (circles). The static limit (filled symbols) is obtained with a quadratic extrapolation.

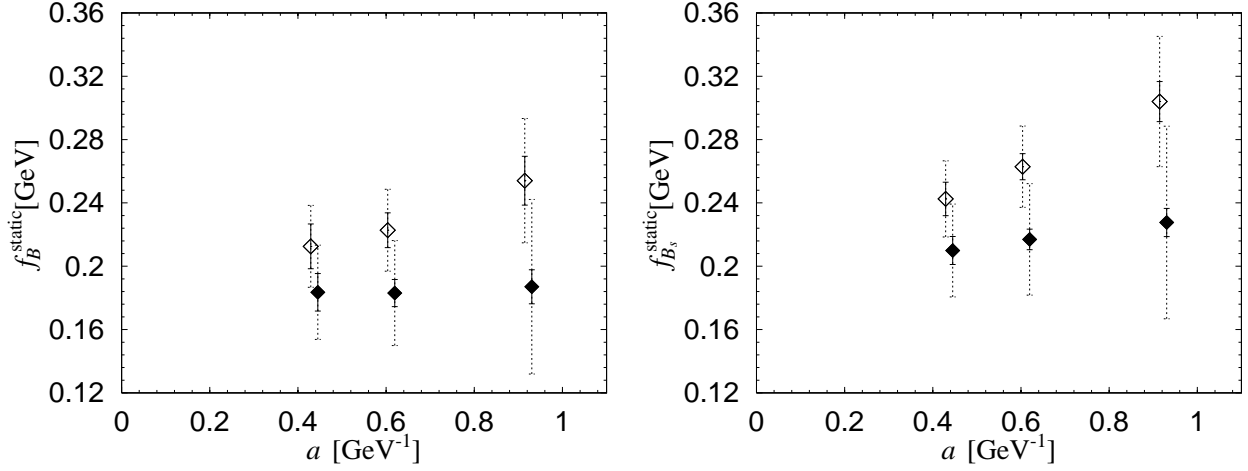


FIG. 8. The lattice spacing dependence of f_B^{static} at $\kappa = \kappa_{\text{crit}}$ (left) and $\kappa = \kappa_{s1}$ (right). Open diamonds represent the result without the operator mixing, while filled diamonds include the mixing effect. The symbols show the q^* averaged results, and are slightly shifted in horizontal axis so that error bars do not overlap. Solid error bars show the statistical error, and dashed ones show the uncertainty of q^* from the difference of the two choices of $q^* = \pi/a$ and $1/a$.

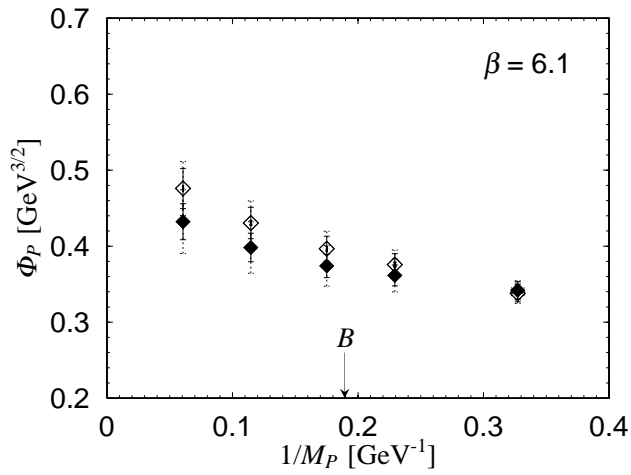
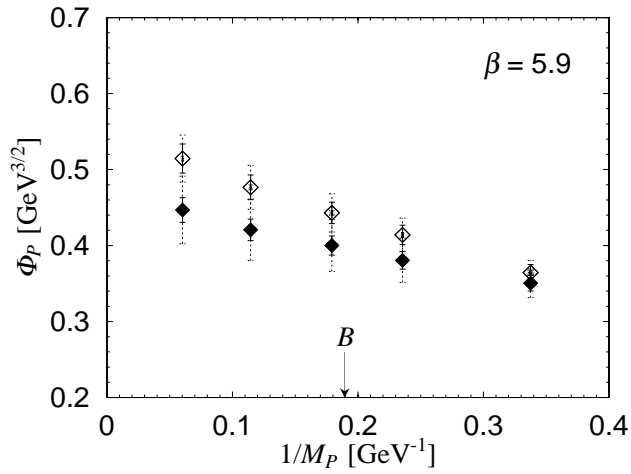
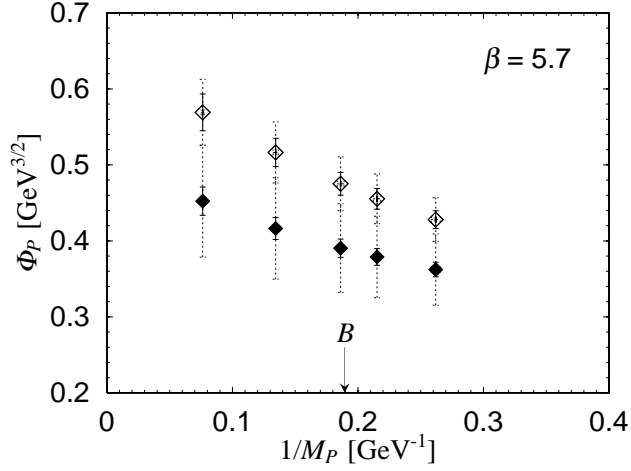


FIG. 9. Φ_P as a function of $1/M_P$ for each β . Open diamonds represent the result without the operator mixing, while filled diamonds include the mixing effect. The symbols show the q^* averaged results. Solid error bars show the statistical error, and dashed ones show the uncertainty of q^* .

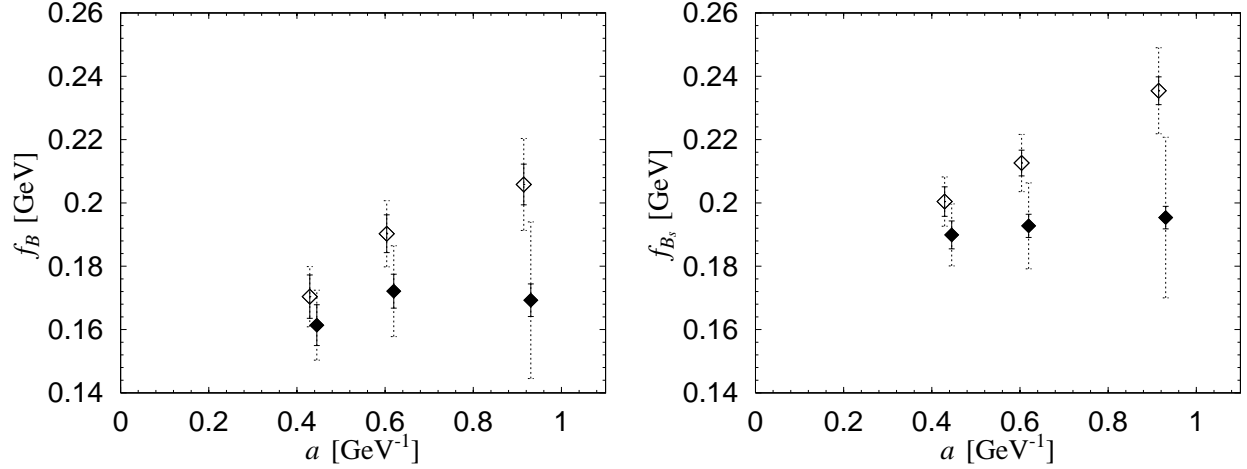


FIG. 10. a dependence of f_B (left) and f_{B_s} (right). Filled symbols represent the result with the contribution from $J_{\text{latt}}^{(1)}$ and $J_{\text{latt}}^{(2)}$. Open symbols do not include these effects. The symbols show the q^* averaged results, and are slightly shifted in horizontal axis so that error bars do not overlap. Solid error bars show the statistical error, and dashed ones show the uncertainty of q^* .

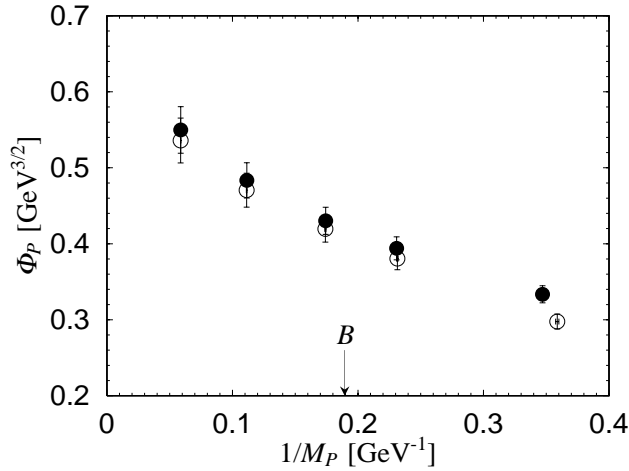


FIG. 11. Comparison of Φ_P from NRQCD-I (filled circles) with that from NRQCD-II (open circles) at tree level.

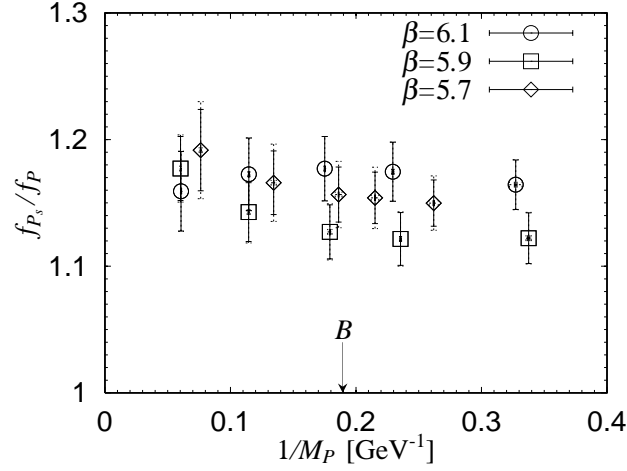


FIG. 12. $1/M_P$ dependence of f_{P_s}/f_P with κ_{s1} . The symbols show the q^* averaged results. Solid error bars show the statistical error, and dotted ones show the uncertainty of q^* .

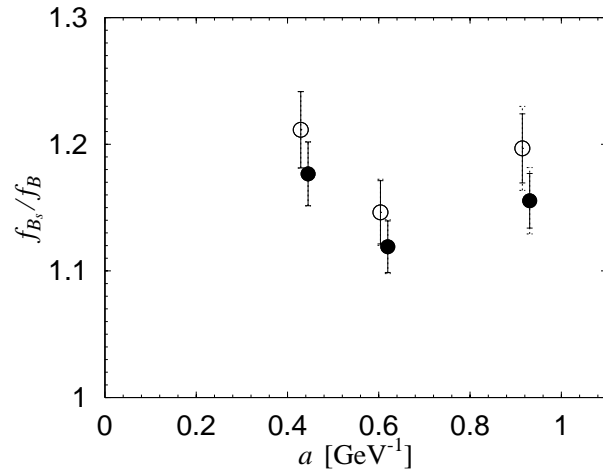


FIG. 13. a dependence of f_{B_s}/f_B with κ_{s1} (filled circles) and with κ_{s2} (open circles). The symbols show the q^* averaged results. Solid error bars show the statistical error, and dotted ones show the uncertainty of q^* .

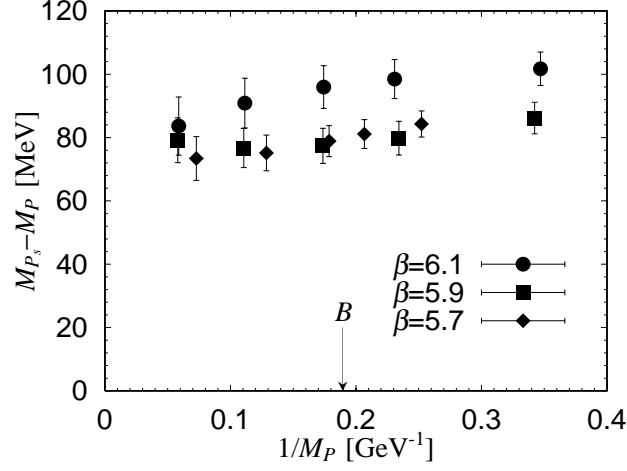


FIG. 14. $1/M_P$ dependence of $M_{P_s} - M_P$ with κ_{s1} . We used the tree level results for $1/M_P$ in the plot.

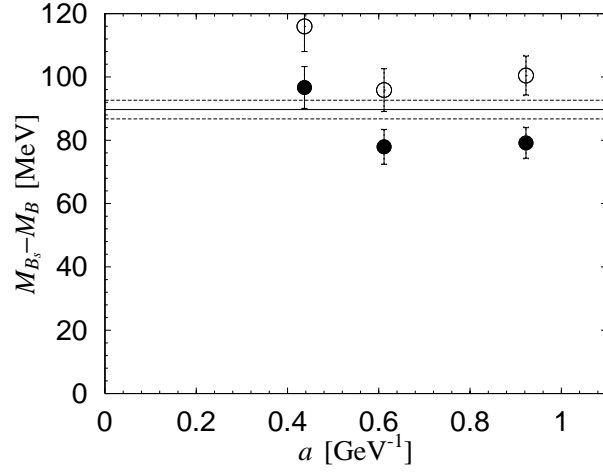


FIG. 15. a dependence of $M_{B_s} - M_B$ with κ_{s1} (filled circles) and with κ_{s2} (open circles). The experimental value is shown by a solid line.

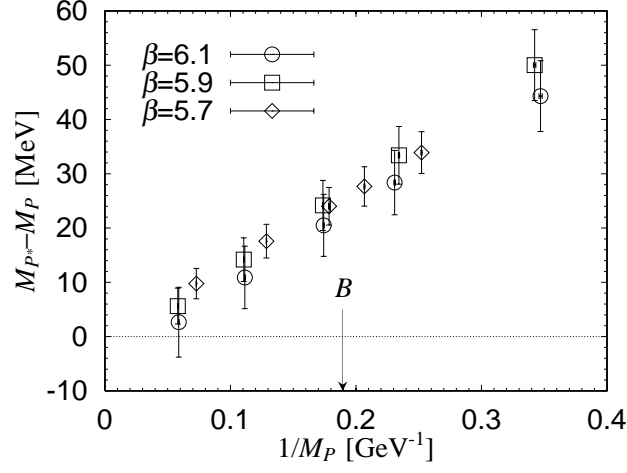


FIG. 16. $1/M_P$ dependence of $M_{P^*} - M_P$. We used the tree level results for $1/M_P$ in the plot.

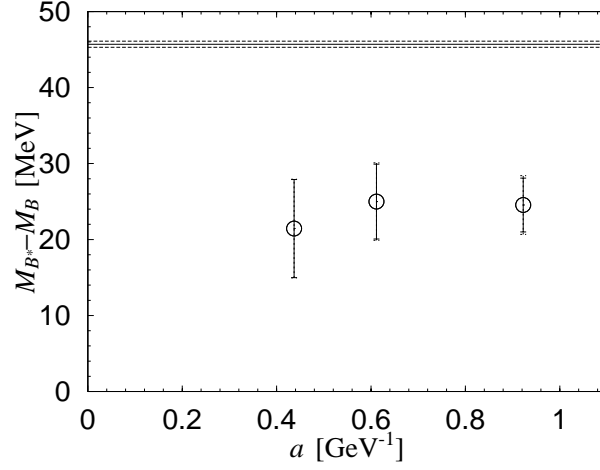


FIG. 17. a dependence of $M_{B^*} - M_B$. The experimental value is shown by a solid line.

TABLES

aM_0	n	$\rho_A^{(0)} - (1/\pi) \log(aM_0)$	$\rho_A^{(1)}/2aM_0$	$\rho_A^{(2)}/2aM_0$	A	B	C
∞	-	-1.317	0.000	1.036	1.069	-	0.481
12.0	2	-1.162	0.026	0.851	1.022	-0.091	0.312
10.0	2	-1.131	0.030	0.809	1.011	-0.075	0.279
7.0	2	-1.061	0.036	0.737	0.983	-0.032	0.197
6.5	2	-1.043	0.037	0.725	0.976	-0.023	0.177
5.0	2	-0.970	0.040	0.656	0.946	0.018	0.094
4.5	2	-0.937	0.039	0.628	0.931	0.036	0.055
3.8	2	-0.876	0.036	0.578	0.903	0.069	-0.014
3.5	2	-0.846	0.034	0.559	0.888	0.086	-0.052
3.0	2	-0.782	0.026	0.516	0.855	0.119	-0.127
2.1	3	-0.626	-0.015	0.442	0.754	0.329	-0.315
1.5	3	-0.433	-0.108	0.378	0.621	0.456	-0.542
1.3	3	-0.341	-0.173	0.360	0.547	0.511	-0.647
0.9	4	-0.088	-0.445	0.374	0.300	0.782	-0.921

TABLE I. One-loop coefficients of the axial vector current $\rho_A^{(0)}$, $\rho_A^{(1)}$ and $\rho_A^{(2)}$ defined in Eq. (9). The self-energy corrections are also listed.

β	6.1	5.9	5.7
size	$24^3 \times 64$	$16^3 \times 48$	$12^3 \times 32$
#conf	120	300	300
c_{sw}	1.525	1.580	1.674
κ	0.13586 0.13642 0.13684 0.13716	0.13630 0.13711 0.13769 0.13816	0.13690 0.13760 0.13840 0.13920
u_0	0.8816	0.8734	0.86087
(aM_0, n)	(7.0,2) (3.5,2) (2.1,2) (1.5,3) (0.9,4)	(10.0,2) (5.0,2) (3.0,2) (2.1,3) (1.3,3)	(12.0,2) (6.5,2) (4.5,2) (3.8,2) (3.0,2)
$\alpha_V(\pi/a)$	0.149	0.164	0.188
$\alpha_V(1/a)$	0.229	0.270	0.355
κ_{crit}	0.13767	0.13901	0.14157
κ_{s1}	0.13635	0.13702	0.13800
κ_{s2}	0.13609	0.13657	0.13707
$1/a$ (GeV)	2.29	1.64	1.08

TABLE II. Lattice parameters.

aM_0	$\kappa = \kappa_{\text{crit}}$			$\kappa = \kappa_{s1}$			$\kappa = \kappa_{s2}$		
	aE^{bin}	$q^* = \pi/a$	$q^* = 1/a$	aE^{bin}	$q^* = \pi/a$	$q^* = 1/a$	aE^{bin}	$q^* = \pi/a$	$q^* = 1/a$
$\beta=5.7$									
12.0	0.669(11)	12.271(11)	11.919(11)	0.737(7)	12.339(7)	11.987(7)	0.755(7)	12.357(7)	12.005(7)
6.5	0.670(10)	6.958(10)	6.770(10)	0.739(6)	7.027(6)	6.839(6)	0.758(5)	7.046(5)	6.858(5)
4.5	0.665(8)	5.021(8)	4.892(8)	0.738(5)	5.093(5)	4.965(5)	0.758(4)	5.113(4)	4.985(4)
3.8	0.663(8)	4.341(8)	4.235(8)	0.737(5)	4.416(5)	4.309(5)	0.757(4)	4.436(4)	4.330(4)
3.0	0.658(7)	3.564(7)	3.481(7)	0.735(4)	3.642(4)	3.559(4)	0.756(4)	3.663(4)	3.580(4)
$\beta=5.9$									
10.0	0.531(8)	10.244(8)	10.058(8)	0.580(5)	10.292(5)	10.106(5)	0.591(5)	10.303(5)	10.117(5)
5.0	0.528(7)	5.389(7)	5.298(7)	0.575(4)	5.435(4)	5.345(4)	0.586(4)	5.446(4)	5.356(4)
3.0	0.522(6)	3.440(6)	3.387(6)	0.569(3)	3.488(3)	3.435(3)	0.580(3)	3.498(3)	3.446(3)
2.1	0.511(6)	2.601(6)	2.594(6)	0.560(3)	2.650(3)	2.643(3)	0.571(3)	2.661(3)	2.654(3)
1.3	0.487(5)	1.806(5)	1.818(5)	0.539(3)	1.859(3)	1.871(3)	0.552(2)	1.871(2)	1.883(2)
$\beta=6.1$									
7.0	0.435(8)	7.255(8)	7.158(8)	0.471(5)	7.292(5)	7.195(5)	0.479(5)	7.299(5)	7.202(5)
3.5	0.423(7)	3.835(7)	3.788(7)	0.462(4)	3.875(4)	3.828(4)	0.470(4)	3.883(4)	3.836(4)
2.1	0.408(6)	2.499(6)	2.494(6)	0.450(3)	2.541(3)	2.535(3)	0.458(3)	2.549(3)	2.544(3)
1.5	0.393(5)	1.903(5)	1.908(5)	0.436(3)	1.946(3)	1.951(3)	0.445(3)	1.954(3)	1.959(3)
0.9	0.359(4)	1.320(4)	1.352(4)	0.404(3)	1.364(3)	1.396(3)	0.413(2)	1.373(3)	1.405(2)

TABLE III. Binding energy and the total mass of the heavy-light pseudoscalar mesons.

aM_0	$\kappa = \kappa_{\text{crit}}$	$\kappa = \kappa_{s1}$	$\kappa = \kappa_{s2}$
$\beta=5.7$			
∞	0.675(41)	0.814(34)	0.851(36)
12.0	0.588(25)	0.693(19)	0.722(20)
6.5	0.531(19)	0.615(13)	0.638(13)
4.5	0.481(15)	0.556(11)	0.575(10)
3.8	0.456(14)	0.527(9)	0.546(9)
3.0	0.421(12)	0.486(8)	0.503(8)
$\beta = 5.9$			
∞	0.312(15)	0.370(11)	0.383(11)
10.0	0.285(11)	0.333(8)	0.344(7)
5.0	0.260(9)	0.296(7)	0.304(7)
3.0	0.235(8)	0.264(5)	0.271(5)
2.1	0.213(7)	0.240(4)	0.246(4)
1.3	0.178(5)	0.201(3)	0.207(3)
$\beta = 6.1$			
∞	0.178(12)	0.205(9)	0.210(8)
7.0	0.159(9)	0.185(7)	0.190(6)
3.5	0.140(7)	0.165(5)	0.170(4)
2.1	0.124(5)	0.148(4)	0.152(3)
1.5	0.114(4)	0.135(3)	0.140(3)
0.9	0.096(3)	0.114(2)	0.118(2)

TABLE IV. Raw data of $a^{3/2}(f_P\sqrt{M_P})^{(0)}$ at κ_{crit} , κ_{s1} and κ_{s2} .

aM_0	$\kappa = \kappa_{\text{crit}}$	$\kappa = \kappa_{s1}$	$\kappa = \kappa_{s2}$
$\beta=5.7$			
∞	-0.485(34)	-0.556(27)	-0.576(29)
12.0	-0.455(22)	-0.511(16)	-0.526(16)
6.5	-0.436(18)	-0.482(12)	-0.495(12)
4.5	-0.415(15)	-0.458(10)	-0.470(10)
3.8	-0.403(14)	-0.446(9)	-0.458(9)
3.0	-0.387(12)	-0.429(8)	-0.441(8)
$\beta = 5.9$			
∞	-0.194(12)	-0.226(8)	-0.234(8)
10.0	-0.189(8)	-0.215(6)	-0.221(5)
5.0	-0.183(7)	-0.203(5)	-0.208(5)
3.0	-0.176(7)	-0.193(4)	-0.198(4)
2.1	-0.170(6)	-0.187(4)	-0.191(4)
1.3	-0.158(5)	-0.176(3)	-0.180(3)
$\beta = 6.1$			
∞	-0.098(8)	-0.111(6)	-0.113(5)
7.0	-0.092(6)	-0.105(4)	-0.108(4)
3.5	-0.086(5)	-0.100(3)	-0.103(3)
2.1	-0.082(4)	-0.097(3)	-0.100(3)
1.5	-0.080(4)	-0.095(2)	-0.098(2)
0.9	-0.079(3)	-0.093(2)	-0.096(2)

TABLE V. Raw data of $2aM_0a^{3/2}(f_P\sqrt{M_P})^{(1)}$ at κ_{crit} , κ_{s1} and κ_{s2} .

	$\beta = 6.1$	$\beta = 5.9$	$\beta = 5.7$
tree	1.903(5)	2.710(6)	4.206(8)
$q^* = \pi/a$	1.913(6)	2.765(6)	4.345(9)
$q^* = 1/a$	1.919(6)	2.804(7)	4.476(9)

TABLE VI. Bare b-quark mass that reproduces the physical B meson mass.

	$\beta = 6.1$			$\beta = 5.9$			$\beta = 5.7$		
	tree	$q^* = \pi/a$	$q^* = 1/a$	tree	$q^* = \pi/a$	$q^* = 1/a$	tree	$q^* = \pi/a$	$q^* = 1/a$
f_B	0.184(7)	0.166(7)	0.157(6)	0.210(6)	0.181(6)	0.163(5)	0.233(7)	0.189(6)	0.150(5)
$f_{B_s} (\kappa_{s1})$	0.215(5)	0.195(5)	0.185(4)	0.233(4)	0.203(4)	0.183(3)	0.265(5)	0.217(4)	0.174(3)
$f_{B_s} (\kappa_{s2})$	0.222(5)	0.201(4)	0.190(4)	0.239(4)	0.208(4)	0.187(3)	0.274(5)	0.225(4)	0.180(3)

TABLE VII. Results for f_B and f_{B_s} in GeV.

	$\beta = 6.1$	$\beta = 5.9$	$\beta = 5.7$
$O(\alpha_s^2)$	3%	5%	12%
$O((a\Lambda_{QCD})^2)$	2%	3%	8%
$O(\alpha_s/(aM)^2)$	6%	4%	2%

TABLE VIII. An order estimate of the possible systematic errors.